

## Article

# Enhancing the Performance of Ceramic-Rich Polymer Composite Electrolytes Using Polymer Grafted LLZO

Pierre Ranque<sup>1</sup>, Jakub Zagórski<sup>1</sup>, Grazia Accardo<sup>1</sup> , Ander Orue Mendizabal<sup>1</sup> , Juan Miguel López del Amo<sup>1</sup>, Nicola Boaretto<sup>1</sup> , Maria Martínez-Ibañez<sup>1</sup> , Hugo Arrou-Vignod<sup>1,2</sup>, Frederic Aguesse<sup>1</sup>, Michel Armand<sup>1</sup> and Shanmukaraj Devaraj<sup>1,\*</sup>

<sup>1</sup> Centre for Cooperative Research on Alternative Energies (CIC energiGUNE), Basque Research and Technology Alliance (BRTA), Alava Technology Park, 01510 Vitoria-Gasteiz, Spain; pranque@cicenergigune.com (P.R.); zagorski.jacob@gmail.com (J.Z.); gaccardo@cicenergigune.com (G.A.); aorue@cicenergigune.com (A.O.M.); jmlopez@cicenergigune.com (J.M.L.d.A.); nboaretto@cicenergigune.com (N.B.); mmartinez@cicenergigune.com (M.M.-I.); harrouvignod@cicenergigune.com (H.A.-V.); faguesse@cicenergigune.com (F.A.); marmand@cicenergigune.com (M.A.)

<sup>2</sup> Department of Applied Chemistry and Science and Technology of Polymeric Materials, Faculty of Chemistry, 20018 San Sebastián, Spain

\* Correspondence: dshanmukaraj@cicenergigune.com



**Citation:** Ranque, P.; Zagórski, J.; Accardo, G.; Orue Mendizabal, A.; López del Amo, J.M.; Boaretto, N.; Martínez-Ibañez, M.; Arrou-Vignod, H.; Aguesse, F.; Armand, M.; et al. Enhancing the Performance of Ceramic-Rich Polymer Composite Electrolytes Using Polymer Grafted LLZO. *Inorganics* **2022**, *10*, 81. <https://doi.org/10.3390/inorganics10060081>

Academic Editors: Christian Julien and Alain Mauger

Received: 3 April 2022

Accepted: 8 June 2022

Published: 13 June 2022

**Publisher's Note:** MDPI stays neutral with regard to jurisdictional claims in published maps and institutional affiliations.



**Copyright:** © 2022 by the authors. Licensee MDPI, Basel, Switzerland. This article is an open access article distributed under the terms and conditions of the Creative Commons Attribution (CC BY) license (<https://creativecommons.org/licenses/by/4.0/>).

**Abstract:** Solid-state batteries are the holy grail for the next generation of automotive batteries. The development of solid-state batteries requires efficient electrolytes to improve the performance of the cells in terms of ionic conductivity, electrochemical stability, interfacial compatibility, and so on. These requirements call for the combined properties of ceramic and polymer electrolytes, making ceramic-rich polymer electrolytes a promising solution to be developed. Aligned with this aim, we have shown a surface modification of Ga substituted  $\text{Li}_7\text{La}_3\text{Zr}_2\text{O}_{12}$  (LLZO), to be an essential strategy for the preparation of ceramic-rich electrolytes. Ceramic-rich polymer membranes with surface-modified LLZO show marked improvements in the performance, in terms of electrolyte physical and electrochemical properties, as well as coulombic efficiency, interfacial compatibility, and cyclability of solid-state cells.

**Keywords:** polymer grafting; composite electrolyte; ceramic-rich; solid-state batteries; LLZO; strategy

## 1. Introduction

Solid-state batteries (SSBs) have attracted great attention in recent years due to their enhanced safety over conventional liquid electrolytes in terms of electrolyte leakage, wide operation temperature, and dendrite growth [1–6]. Polymer electrolytes offer advantages of cost-effective processing, design flexibility, and good adhesion to the electrodes [7–9]. However, solvent-free polymer electrolytes have inherent low ionic conductivity at room temperature and do not offer sufficient mechanical resistance to dendrites growth. A combination of both polymer and ceramic electrolytes seems to be the best solution to overcome the issues addressed [10–15]. Researchers are interested in bringing the advantages of ceramic electrolytes into polymer electrolytes, “ceramic-rich electrolytes”. Ceramic-rich electrolyte membrane preparation is apparently simple but numerous practical difficulties need to be addressed when trying to develop homogenous membranes [16]. The homogeneity is affected by the agglomeration of particles or phase separation of the ceramic in the polymer matrix [17]. Homogeneous particles distribution is quite difficult to achieve and, as a result, the performance of the electrolyte membranes is affected in terms of ionic conductivity, mechanical stability, and cell performance. An approach to obtain more homogenous ceramic-rich membranes could be to ease the dispersion of particles during the mixing process [18]. For this purpose, the grafting of polymer chains on the surface of the

inorganic particles can be an effective method, as was previously seen on non-conductive fillers [19–23].

In this paper, we focus on a composite of polyethylene oxide (PEO) and Ga substituted  $\text{Li}_7\text{La}_3\text{Zr}_2\text{O}_{12}$  (LLZO), since this combination is considered as very promising for solid electrolytes [16,24–35]. Indeed, with suitable dopants, LLZO crystallizes in a cubic phase that has a high ionic conductivity at room temperature ( $\sigma_{\text{bulk}} \approx 10^{-3} \text{ S cm}^{-1}$ ) [36,37] and can be used within a wide voltage window [2,38]. Bringing together the properties of LLZO and PEO in ceramic-rich electrolytes could result in hybrid electrolytes with high ionic conductivity, good mechanical properties, good interfacial contact as well as high processability [39]. Herein, surface modification of the LLZO garnets has been attempted using phosphonic acid-terminated poly(ethylene glycol) (PEG), and its effect on the fabrication and properties of ceramic-rich polymer composite electrolytes is studied in detail.

## 2. Results and Discussion

The exceptional binding properties of phosphonic acid onto oxide surfaces [40] was the prime motivation for using phosphonic acid terminated PEG. Phosphonic acid-based surface modification of LLZO particles was carried out as shown in Figure 1. The phosphonic acid terminated PEG is expected to bind on the surface of the LLZO particles either by mono-, bi-, or tridentate coordination. The most probable coordination mode (bidentate) has been depicted in Figure 1.

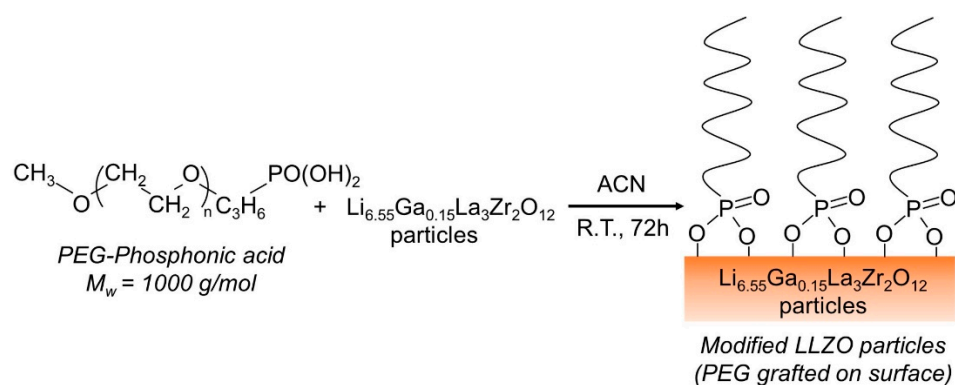


**Figure 1.** Schematic of the polymer grafting process on LLZO particles.

The surface-grafted LLZO particles were analyzed initially by FT-infrared spectroscopy. Figure 2a shows the comparison of the starting phosphonic acid terminated PEG, bare LLZO, and the surface-grafted LLZO. Following the evolution of the two prominent vibrational bands of PEG, namely C-H stretching and C=O stretching, the presence of PEG on the surface-modified LLZO particles can be detected. Furthermore, thermogravimetric measurements show a mass loss of 8.3% in the surface-modified LLZO (Figure 2b), which was not observed with bare LLZO, thus confirming the presence of PEG molecules on the surface of LLZO. Although the presence of PEG has been detected we further used solid-state NMR spectroscopy to detect the presence of phosphonic acid terminal end group.  $^{31}\text{P}$  solid-state NMR shift is shown in Figure 2c, where the shift due to the presence of  $\text{PO}_3^{2-}$  was observed, thus confirming the grafting of the PEG molecule with terminal phosphonic acid grafted onto the surface of LLZO particles.

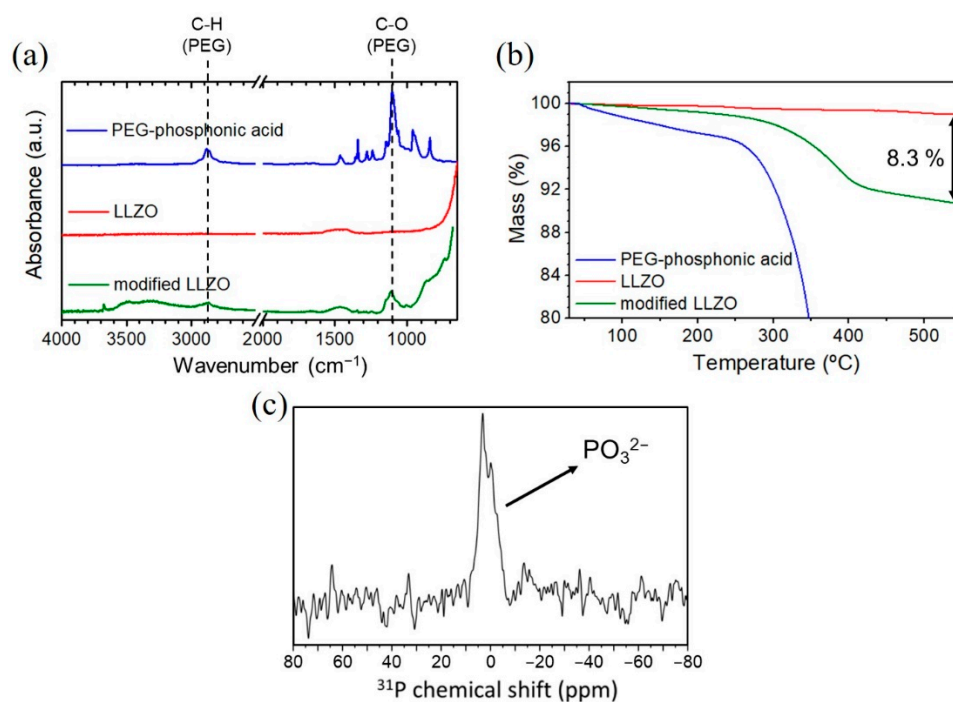


**Figure 2.** (a) FTIR characterization of PEG-phosphonic acid, pristine LLZO, and modified LLZO. (b) TGA of PEG-phosphonic acid, pristine LLZO, and modified LLZO. (c) Solid-state NMR <sup>31</sup>P 1D spectrum of the modified LLZO.

X-ray diffraction spectra of the LLZO show no changes in the garnet structure due to the surface modification (Figure S1a) and the presence of PEO/PEG was detected as a hump between 15 to 20° (2θ value) indicated by the region of the green circle for the modified garnets whereas no humps were observed for the unmodified garnets. The particle size of the garnets used for preparing the composites was ≈2.23 μm determined using SEM (Figure S1b) with an ionic conductivity of  $5.88 \times 10^{-2}$  mS/cm at RT and  $4.41 \times 10^{-1}$  mS/cm at 70 °C (Figure S1c). The major focus of this work is to enable the preparation of homogeneous ceramic-rich LLZO-containing membranes, that is normally hindered due to factors such as aggregation of the LLZO particles, inhomogeneous distribution of the particles on the surface of the polymer matrix, and inhomogeneous distribution throughout the thickness of the polymer matrix. Improvements on these three factors are a requisite when high loadings (ceramic-rich) of LLZO particles are incorporated into the polymer membranes.

Polymer membranes with a high amount of LLZO were prepared (30 vol%) and visual examination of the membranes was carried out (Figure 3a). The membranes with unmodified LLZO particles have a lighter color when compared to the modified LLZO incorporated membranes. This suggests an irregular distribution of the LLZO particles along the surface of the membranes. Optical microscopic images of the membranes (Figure S2), show a dense distribution of the ceramic particles at the surface of the modified-LLZO membrane, while lower distribution density was observed for the bare-LLZO membrane. To further confirm, SEM morphology analysis of the membranes was performed. Figure 3b shows a ceramic-rich surface in the case of modified-LLZO incorporated membrane whereas a scanty distribution of the LLZO particles was observed on the surface of the polymer membranes with unmodified-LLZO. Higher magnification images indicate particles segregation with unmodified LLZO, which leads to a particle-particle contact, while this is clearly not the case with modified-LLZO membranes. These results suggest that better quality membranes can be achieved by grafting PEG-terminated phosphonic acid on the LLZO particles. It is also worth noting that the DSC profiles of the polymer electrolytes polyethylene oxide: lithium bis (trifluoromethylsulfonyl) imide (PEO:LiTFSI) prepared

with the 30 vol% modified- and unmodified-LLZO are similar, with a melting temperature  $T_m$  of  $\approx 64$  °C and a glass transition temperature  $T_g$  of  $\approx -32$  °C (Figure S3) in both cases.

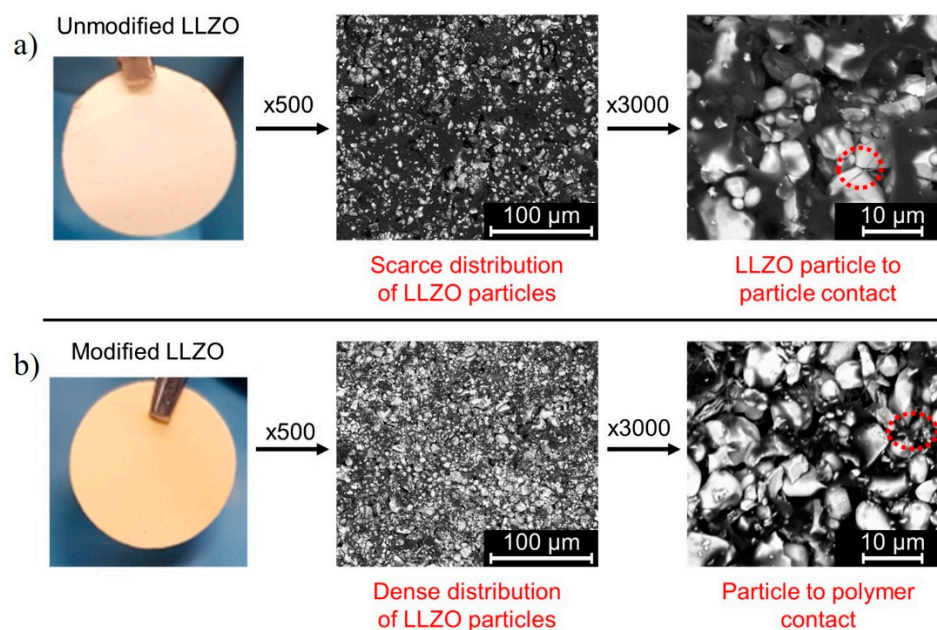


**Figure 3.** Surface morphology characterizations of the composite membranes: (a) PEO:LiTFSI + 30 vol% LLZO (from left to right: photography, SEM at a magnitude of 500 $\times$  and 3000 $\times$ ), and (b) PEO:LiTFSI + 30 vol% modified LLZO (from left to right: photography, SEM at a magnitude of 500 $\times$  and 3000 $\times$ ).

Electrochemical characterization of the modified- and unmodified-LLZO ceramic-rich polymer membranes was performed to evaluate their performance with respect to the morphology of the polymer membranes. Temperature-dependent ionic conductivity analysis (Figure 4a) obtained by AC impedance spectroscopy shows a slight improvement in the ionic conductivity with the modified-LLZO membranes, which have an ionic conductivity value of  $1.3 \times 10^{-6}$ ,  $3.8 \times 10^{-5}$ , and  $1.1 \times 10^{-4}$  S cm $^{-1}$  in comparison with  $8.6 \times 10^{-7}$ ,  $1.6 \times 10^{-5}$ , and  $7.8 \times 10^{-5}$  S cm $^{-1}$  for unmodified ones at 25, 50, and 70 °C, respectively. The activation energy was analyzed (Figure S4a) and two regions were observed, one from RT to 60 °C and another from 60 °C to 80 °C. This correlates with the melting point of PEO above 60 °C. The activation energies were calculated to be 1.03 eV and 0.3 eV ( $\pm 0.05$  eV) for modified garnet composites and 0.96 eV and 0.4 eV ( $\pm 0.05$  eV) for the unmodified composites below and above 60 °C. The improvement in the interfacial resistance can be seen from the Nyquist plot at 25 °C shown in Figure 4b with the fitted curve (zoomed) shown as inset. The corresponding equivalent circuit is shown in Figure S4b. The minor enhancement in ionic conductivity observed with modified-LLZO is due to the more homogeneous particle distribution as the crystallinity of the polymer remains unaffected, as seen from the DSC curves. In addition to the 30 vol% LLZO membranes, to further explore the effects of LLZO grafting on the membranes properties, two additional membranes were prepared with (a) a lower content of LLZO (10 vol%) and (b) a very high content of LLZO (70 vol%) with both modified and unmodified particles. Figure S4c shows that the difference in ionic conductivity between the modified and unmodified membranes is negligible at 10 vol%, whereas a marked difference in the ionic conductivity is observed at high LLZO concentration (70 vol%). This suggests that the surface modification plays an important role in preparing ceramic-rich membranes.

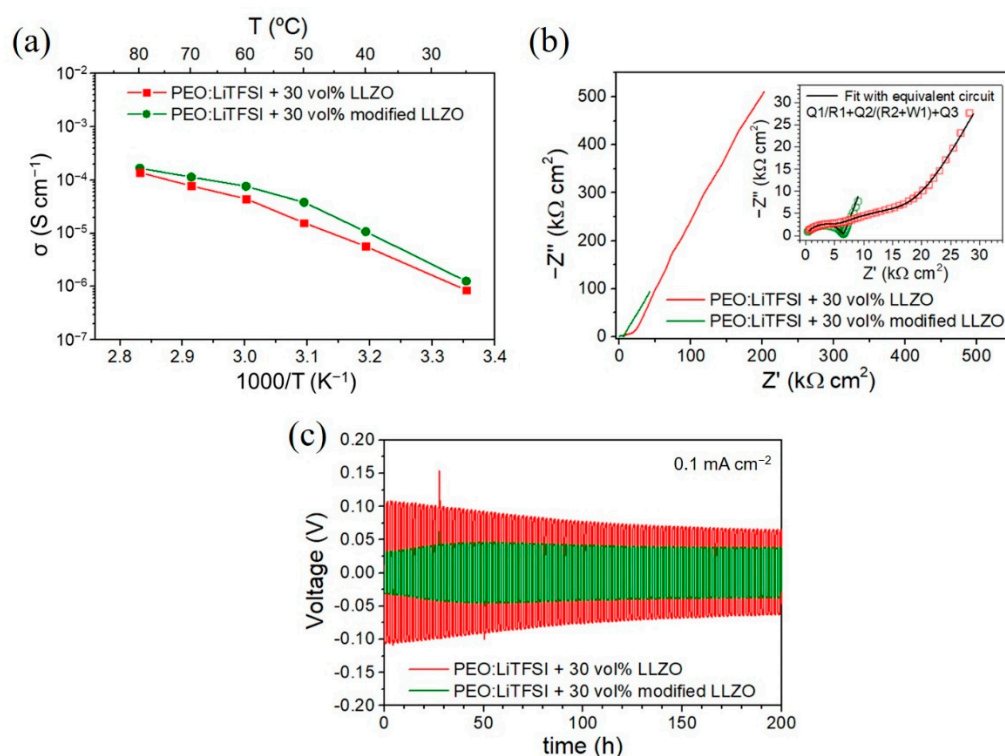


**Figure 4.** Electrochemical characterizations of the composite membranes PEO:LiTFSI + 30 vol% LLZO with (a) Arrhenius plots, (b) Nyquist plots at 25 °C, and (c) plating/stripping measurements at 70 °C.

In order to test the compatibility of the ceramic-rich membranes with Li metal, plating-stripping tests were carried out in Li-symmetric cells. An average overpotential of 35 mV was observed with the modified-LLZO polymer membranes (Figure 4c), whereas an overvoltage of 70 mV was obtained with unmodified-LLZO membranes. More pronounced effects were observed in the case of 10 vol% incorporated membranes with and without modification (Figure S4d) with an overpotential of 180 mV for the unmodified-LLZO and 44 mV with modified-LLZO membranes. This improvement is attributed to the better distribution of modified-LLZO particles in the polymer matrix, contributing to lowering the resistance at the Li/ Polymer/Li interface. Instability issues between LLZO pellets and Li metal have been shown in [41], however, in our current work, the LLZO particles are incorporated in the polymer matrix, and they are not directly in contact with the lithium metal anode (PEO in the case of unmodified ceramic and PEO/PEG in the case of modified ceramic). Therefore, possible instability effects are considerably reduced and are practically not observed.

Li transference numbers were determined using Bruce Vincent technique [42] as shown in Figure S4e. The transference numbers were found to be in both cases  $\ll 1$  but a marked improvement is seen in the case of modified composites (0.2) when compared to unmodified composites (0.14). The electrochemical stability of the composites was also investigated using linear sweep voltammetry (Figure S4f). Similar stability values  $\approx 5$  V was observed for both the composites with a small increase in the current at 4.2 V for the surface modified composites that could be attributed to the presence of low molecular weight PEG.

The cell performance of ceramic-rich membranes with modified and unmodified-LLZO were tested with  $\text{LiFePO}_4$  as cathode and Li metal anodes (Figure 5a,b). An initial capacity of 150 and 118  $\text{mAhg}^{-1}$  was observed with modified and unmodified-LLZO, respectively (Figure 5a). The capacity retention after 100 cycles was of 146  $\text{mAhg}^{-1}$  for the modified-LLZO based electrolytes, and 32  $\text{mAhg}^{-1}$  for unmodified-LLZO electrolytes. The voltage profiles of the cells at the 1st, 25th, 50th, and 100th cycles (Figure 5c,d) are also shown for a better understanding. The coulombic efficiency was close to 100% for

the modified-LLZO electrolytes, whereas strong fluctuations (with the lowest value of 6.8%) were observed between the cycles 19 and 31 with the unmodified-LLZO electrolyte (Figure 5b). By average, the coulombic efficiency was lower with unmodified-LLZO particles than with modified LLZO. The galvanostatic cycling behavior is also well evidenced by the voltage profiles shown in Figure 5c,d, which shows a poor capacity retention for the unmodified-LLZO electrolytes. The high capacity observed in the charge curve with voltage fluctuations at the 25th cycle is attributed to the formation of dendrites in the unmodified composites. Further, the formed dendrites break, leading to normal cycling for the consecutive cycles. This is related to the inhomogeneous ceramic particle distribution in the case of unmodified composites that leads to uneven  $\text{Li}^+$  diffusion through the composite membrane. The increase in the capacity, compared to the initial cycles, is due to the formation of better solid electrolyte interface (SEI) for consecutive cycles, that leads to better specific capacity and charge/discharge capacity retention.

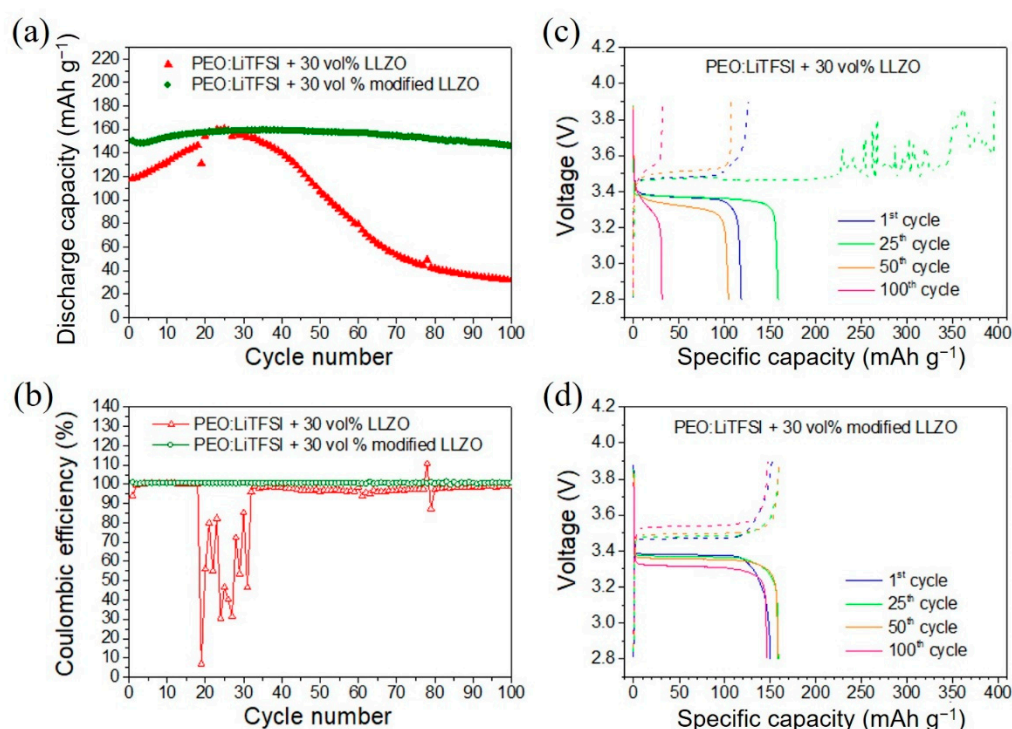


**Figure 5.** Galvanostatic cycling at 0.1C of  $\text{LiFePO}_4/\text{Carbon Black}/\text{PEO}:\text{LiTFSI}$  cathodes vs. Li metal anode, using PEO:LiTFSI + 30 vol% LLZO membranes. (a) Specific discharge capacity upon cycling, (b) coulombic efficiency upon cycling, (c) charge/discharge curves of the 1st, 25th, 50th, and 100th cycles of unmodified-LLZO electrolyte, and (d) charge/discharge curves of the 1st, 25th, 50th, and 100th cycles of modified-LLZO electrolyte.

In order to obtain a deeper understanding of the cycling behavior, a postmortem analysis was carried out after 100 cycles. A cross sectional analysis of the cell is shown in Figure 6.

The SEM images show that in unmodified-LLZO electrolytes, the LLZO particles tend to agglomerate and segregate unevenly throughout the thickness of the cells. On the other hand, the modified-LLZO particles tend to uniformly distribute throughout the thickness of the electrolyte. This is due to the uniform polymer layer that was grafted on to the surface of the LLZO particles preventing particle agglomeration and allowing better particle distribution. This in turn leads to a better interfacial contact between the Li metal electrodes for the cells containing modified-LLZO particle loaded electrolyte membranes.

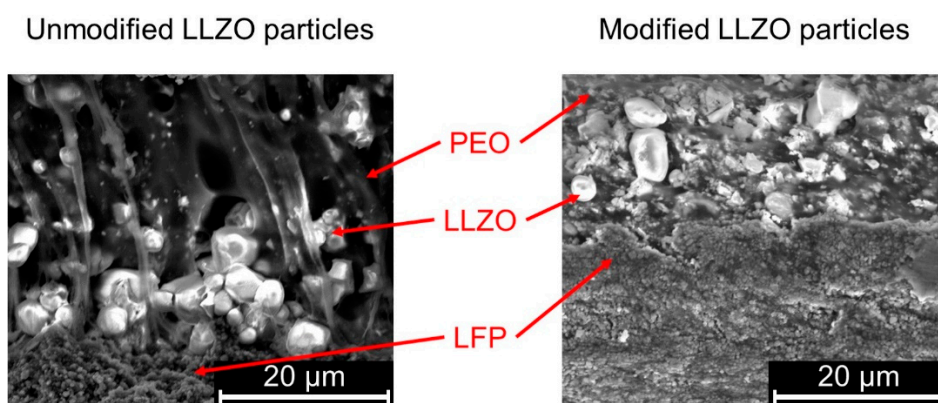


**Figure 6.** Postmortem analysis of the LFP half cells after 100 cycles by SEM, at a magnitude of 5500 $\times$ . Unmodified-LLZO composite on the left and modified-LLZO on the right.

### 3. Experimental Section

#### 3.1. Synthesis of Cubic-LLZO

Ga-substituted LLZO ( $\text{Li}_{6.55}\text{Ga}_{0.15}\text{La}_3\text{Zr}_2\text{O}_{12}$ ) was synthesized using a citric acid-nitrate route [36,43]. First,  $\text{Ga}_2\text{O}_3$  ( $\geq 99.99\%$ , Sigma Aldrich) was digested at 180  $^\circ\text{C}$  in  $\text{HNO}_3$ , then  $\text{La}(\text{NO}_3)_3 \cdot 6\text{H}_2\text{O}$  ( $\geq 99.99\%$ , Sigma Aldrich),  $\text{Zr}(\text{C}_5\text{H}_7\text{O}_2)_4$  ( $>98\%$ , Alfa Aesar), and  $\text{LiNO}_3$  ( $>99.0\%$ , Sigma Aldrich) were mixed one by one in stoichiometric quantities (with a 10% Li excess) in a small amount of water until the full dissolution. Citric acid monohydrated ( $>99.0\%$ , Sigma-Aldrich) was added to the solution as a chelating agent and the resulting solution was heated up to 70  $^\circ\text{C}$  under stirring until the formation of a yellow gel. The solvent was slowly evaporated in a sand bath and the organic components were then burned off at 600  $^\circ\text{C}$  for 12 h. The resulting powder was ground and reheated to 950  $^\circ\text{C}$  for 12 h in dry  $\text{O}_2$  to obtain a pure cubic phase.

#### 3.2. LLZO Surface Grafting (Modified LLZO)

LLZO surface grafting was carried out in a glovebox by stirring 0.565 g of LLZO with 0.435 g of phosphonic acid-terminated poly(ethylene glycol) ( $1000 \text{ g mol}^{-1}$ , Specific Polymers France) in acetonitrile (ACN). The reaction was carried out for 72 h at room temperature. The modified LLZO was recovered after subsequent washing with ACN and dried in a vacuum oven attached to the glove box at 50  $^\circ\text{C}$  for 12 h.

#### 3.3. X-ray Diffraction

Powder X-ray diffraction (PXRD) patterns were recorded on a Bruker D8 Discover X-ray diffractometer, using  $\lambda_{\text{Cu-K}\alpha 1} = 1.54056 \text{ \AA}$  radiation in the  $2\theta$  range from 2  $^\circ\text{C}$  to 80  $^\circ\text{C}$  with a step width of 0.0198  $^\circ\text{C}$ .

#### 3.4. Solid-State Nuclear Magnetic Resonance Spectroscopy (ss-NMR)

The sample was prepared by firmly packing the modified LLZO powder in a 2.5 rotor. Magic Angle Spinning Nuclear Magnetic Resonance (MAS NMR) was performed using a Bruker Avance III 500 spectrometer and a Top Spin software. The spectrum was recorded at a rotor spinning at the magic angle (MAS frequency) of 20 kHz.

#### 3.5. Preparation of Polymer Electrolyte Membranes

Free standing polymer electrolytes were prepared in a glovebox under an inert atmosphere (Mbraun under Argon  $< 1 \text{ ppm O}_2, \text{H}_2\text{O}$ ) as follows: PEO ( $5\text{M g mol}^{-1}$ ) and LiTFSI (Sigma Aldrich) were dissolved in ACN. LLZO (synthesized via citrate route) was added to the solution. After stirring the suspension for 12 h, the solvent was slowly evaporated at room temperature (48 h) and the evaporation of the solvent was completed by applying high vacuum at 50  $^\circ\text{C}$  for 12 h.

### 3.6. Thermal Behavior

The thermal property of the samples was studied using thermogravimetric analysis (TGA) and differential scanning calorimetry (DSC). TGA was performed on a TGA 209 F1 Libra (Netzsch). Samples of ~5 mg were heated from room temperature to 550 °C at a heating rate of 10 °C min<sup>-1</sup> under argon flow. DSC was performed on a DSC 2500 differential calorimeter (TA Instruments) by placing samples of ~5 mg in sealed aluminum pans. The samples were first heated at a rate of 10 °C min<sup>-1</sup>, from 25 °C to 150 °C, and were left for 5 min at 150 °C to avoid the influence of thermal history, in order to be able to compare the crystallization/melting temperature. The samples then undergo a cooling ramp down to -80 °C at a rate of 10 °C min<sup>-1</sup>, and are subsequently heated to 150 °C at 10 °C min<sup>-1</sup> after a hold period at -80 °C for 5 min.

### 3.7. Ionic Conductivity

The ionic conductivity ( $\sigma$ ) of the polymer electrolytes was determined by AC impedance spectroscopy using a VMP3 potentiostat (Biologic®, Claix, France). The frequency ranged from 100 mHz to 1 MHz with a signal amplitude of 10 mV. All cells (CR2032 type) were assembled in an argon-filled glove box (Mbraun < 1 ppm O<sub>2</sub>, H<sub>2</sub>O), using two stainless steel blocking electrodes. The conductivities were analyzed in a temperature range from 25 °C to 80 °C (with a preheating at 80 °C).

### 3.8. Electrochemical Stability vs. Li Electrode

Lithium plating/stripping studies were carried out using a Maccor Battery Tester (Series 4000). Symmetric cells were prepared by sandwiching the electrolytes between two lithium disks in CR2032 cell configuration. The cells were cycled at 70 °C with a current density of 0.1 mA cm<sup>-2</sup> during for 1 h per half cycle.

### 3.9. Anodic Stability

Linear sweep voltammetry (LSV) was performed on CR2032 cells, comprising stainless steel working electrode and Li0 disk as both counter and reference electrode. All LSV measurements were performed between the open circuit voltage (OCV) and 6.0 V vs. Li/Li<sup>+</sup> at a scan rate of 1 mV s<sup>-1</sup>.

### 3.10. Li-Ion Transference Number

Li-ion transference number of the membranes was measured with a Biologic potentiostat at 70 °C. The electrolytes were sandwiched between two non-blocking electrodes (lithium disks) in CR2032 cells. The combination of alternating-current (AC) impedance and direct-current (DC) polarization measurements suggested by Bruce-Vincent [42] were employed for obtaining the Li<sup>+</sup> transference numbers.

### 3.11. Cathode Preparation

The cathode was composed with 63 wt% LFP (LiFePO<sub>4</sub>, Aleees, China) as active material, 7 wt% conductive carbon (C65, Timcal) and 30 wt% PEO:LiTFSI (EO/Li = 20) as binder. The slurry was cast on aluminum current collector using the doctor blade technique, followed by vacuum drying at 50 °C for 12 h. The areal capacity of the final cathode was around 0.63 mAh cm<sup>-2</sup>.

### 3.12. Full Cells Measurements

Galvanostatic cycling of solid-state Li metal solid-state batteries were carried out using Maccor Battery Tester (Series 4000). Composite electrolytes were sandwiched between a lithium metallic disk and LFP cathode (LFP/carbon black/PEO:LiTFSI, 63/7/30 wt%) in a CR2032 coin cell configuration assembled in an argon-filled glove box and cycled at 70 °C at a C-rate of 0.1C between 2.8 V and 4.2 V.

#### 4. Conclusions

Ceramic-rich electrolytes represent a promising solution for future solid-state batteries, as they incorporate the advantages of both polymers and ion conducting ceramics into the electrolytes. This is often not easy due to factors such as particle agglomeration and non-uniform dispersion, leading to poor performance of ceramic-rich electrolytes. We have tried to tackle this issue by surface modification of Li-ion conducting moisture sensitive fillers, LLZO, with phosphonic acid-terminated PEG. The latter binds to the oxide surfaces creating a monolayer of the polymer surface. We have shown from our results that LLZO surface modification contributes to high quality membranes with uniform distribution of particles throughout the matrix, thus enhancing the property of the ceramic-rich electrolyte membranes. The surface grafting results in better interfacial contact, better cyclability and in higher ionic conductivity of the polymer membranes, thus making it a feasible technique for practical application in solid-state Li metal batteries.

**Supplementary Materials:** The following supporting information can be downloaded at: <https://www.mdpi.com/article/10.3390/inorganics10060081/s1>, Figure S1: (a) Powder X-ray diffraction patterns of the pure cubic Ga-substituted LLZO ( $\text{Li}_{6.55}\text{Ga}_{0.15}\text{La}_3\text{Zr}_2\text{O}_{12}$ ) powder without (top) and with (bottom) grafted PEG showing the presence of PEG (green circles) in the grafted LLZO; (b) SEM image of the LLZO particles and (c) Nyquist plot of LLZO pellet taken at RT and 70 °C with Li electrodes. Title; Figure S2: Optical microscope images of PEO:LiTFSI + 30 vol% LLZO membranes without (left) and with (right) LLZO modification, Figure S3: Differential scanning calorimetry curves of PEO:LiTFSI + 30 vol% LLZO (left) and PEO:LiTFSI + 30 vol% modified LLZO (right), Figure S4: (a) Arrhenius plots of PEO:LiTFSI + 30 vol% LLZO composite membranes with the corresponding activation energies above and below PEO:LiTFSI (20:1) melting point (60 °C); (b) equivalent circuit and resistances calculated by fitting for Nyquist plots at 25 °C of PEO:LiTFSI + 30 vol% unmodified and modified LLZO electrolytes; (c) Arrhenius plots of 10 and 70 vol% LLZO composite membranes; (d) Plating/stripping measurements of 10 vol% LLZO composite membranes at 70 °C; (e) Li-ion transference number ( $t_{\text{Li}^+}$ ) measurements of PEO:LiTFSI + 30 vol% LLZO (up) and PEO:LiTFSI + 30 vol% modified LLZO (down) at 70 °C; (f) Linear sweep voltammetry curves of PEO:LiTFSI + 30 vol% LLZO composite membranes at 70 °C.

**Author Contributions:** Conceptualization, M.A. and S.D.; methodology, S.D. and P.R.; validation, S.D., P.R. and M.A.; formal analysis, S.D., P.R. and M.A.; investigation, P.R., S.D., J.M.L.d.A., J.Z., G.A., A.O.M. and N.B.; data curation, S.D., P.R. and H.A.-V.; writing—original draft preparation, S.D., P.R. and H.A.-V., writing—review and editing, S.D., M.A., H.A.-V., P.R., N.B., M.M.-I., J.M.L.d.A., G.A., A.O.M. and F.A.; supervision, S.D. and M.A. All authors have read and agreed to the published version of the manuscript.

**Funding:** This research received no external funding.

**Institutional Review Board Statement:** Not applicable.

**Informed Consent Statement:** Not applicable.

**Data Availability Statement:** Not applicable.

**Acknowledgments:** The authors would like to acknowledge the financial support from CIC Energi güne.

**Conflicts of Interest:** The authors declare no competing financial interest.

#### References

1. Gür, T.M. Review of electrical energy storage technologies, materials and systems: Challenges and prospects for large-scale grid storage. *Energy Environ. Sci.* **2018**, *11*, 2696–2767. [[CrossRef](#)]
2. Li, M.; Wang, C.; Chen, Z.; Xu, K.; Lu, J. New Concepts in Electrolytes. *Chem. Rev.* **2020**, *120*, 6783–6819. [[CrossRef](#)]
3. Wang, Q.; Wang, H.; Wu, J.; Zhou, M.; Liu, W.; Zhou, H. Advanced electrolyte design for stable lithium metal anode: From liquid to solid. *Nano Energy* **2021**, *80*, 105516. [[CrossRef](#)]
4. Chen, J.; Wu, J.; Wang, X.; Zhou, A.a.; Yang, Z. Research progress and application prospect of solid-state electrolytes in commercial lithium-ion power batteries. *Energy Storage Mater.* **2021**, *35*, 70–87. [[CrossRef](#)]
5. Mauger, A.; Julien, C.M.; Paolella, A.; Armand, M.; Zaghib, K. Building Better Batteries in the Solid State: A Review. *Materials* **2019**, *12*, 3892. [[CrossRef](#)]

6. Manthiram, A.; Yu, X.; Wang, S. Lithium battery chemistries enabled by solid-state electrolytes. *Nat. Rev. Mater.* **2017**, *2*, 16103. [[CrossRef](#)]
7. Wang, H.; Sheng, L.; Yasin, G.; Wang, L.; Xu, H.; He, X. Reviewing the current status and development of polymer electrolytes for solid-state lithium batteries. *Energy Storage Mater.* **2020**, *33*, 188–215. [[CrossRef](#)]
8. Fan, L.; Wei, S.; Li, S.; Li, Q.; Lu, Y. Recent Progress of the Solid-State Electrolytes for High-Energy Metal-Based Batteries. *Adv. Energy Mater.* **2018**, *8*, 1702657. [[CrossRef](#)]
9. Forsyth, M.; Porcarelli, L.; Wang, X.; Goujon, N.; Mecerreyes, D. Innovative Electrolytes Based on Ionic Liquids and Polymers for Next-Generation Solid-State Batteries. *Acc. Chem. Res.* **2019**, *52*, 686–694. [[CrossRef](#)]
10. Li, S.; Zhang, S.Q.; Shen, L.; Liu, Q.; Ma, J.B.; Lv, W.; He, Y.B.; Yang, Q.H. Progress and Perspective of Ceramic/Polymer Composite Solid Electrolytes for Lithium Batteries. *Adv. Sci.* **2020**, *7*, 1903088. [[CrossRef](#)]
11. Tang, S.; Guo, W.; Fu, Y. Advances in Composite Polymer Electrolytes for Lithium Batteries and Beyond. *Adv. Energy Mater.* **2020**, *11*, 2000802. [[CrossRef](#)]
12. Zhang, T.; He, W.; Zhang, W.; Wang, T.; Li, P.; Sun, Z.; Yu, X. Designing composite solid-state electrolytes for high performance lithium ion or lithium metal batteries. *Chem. Sci.* **2020**, *11*, 8686–8707. [[CrossRef](#)]
13. Zhang, D.; Xu, X.; Qin, Y.; Ji, S.; Huo, Y.; Wang, Z.; Liu, Z.; Shen, J.; Liu, J. Recent Progress in Organic-Inorganic Composite Solid Electrolytes for All-Solid-State Lithium Batteries. *Chemistry* **2020**, *26*, 1720–1736. [[CrossRef](#)]
14. Cheng, Z.; Liu, T.; Zhao, B.; Shen, F.; Jin, H.; Han, X. Recent advances in organic-inorganic composite solid electrolytes for all-solid-state lithium batteries. *Energy Storage Mater.* **2021**, *34*, 388–416. [[CrossRef](#)]
15. Yu, X.; Manthiram, A. A review of composite polymer-ceramic electrolytes for lithium batteries. *Energy Storage Mater.* **2021**, *34*, 282–300. [[CrossRef](#)]
16. Zagórski, J.; del Amo, J.M.L.; Cordill, M.J.; Aguesse, F.; Buannic, L.; Llordés, A. Garnet–Polymer Composite Electrolytes: New Insights on Local Li-Ion Dynamics and Electrodeposition Stability with Li Metal Anodes. *ACS Appl. Energy Mater.* **2019**, *2*, 1734–1746. [[CrossRef](#)]
17. Bonilla, M.R.; Daza, F.A.G.; Ranque, P.; Aguesse, F.; Carrasco, J.; Akhmatskaya, E. Unveiling Interfacial Li-Ion Dynamics in Li<sub>7</sub>La<sub>3</sub>Zr<sub>2</sub>O<sub>12</sub>/PEO(LiTFSI) Composite Polymer-Ceramic Solid Electrolytes for All-Solid-State Lithium Batteries. *ACS Appl. Mater. Interfaces* **2021**, *13*, 30653–30667. [[CrossRef](#)]
18. Kango, S.; Kalia, S.; Celli, A.; Njuguna, J.; Habibi, Y.; Kumar, R. Surface modification of inorganic nanoparticles for development of organic–inorganic nanocomposites—A review. *Prog. Polym. Sci.* **2013**, *38*, 1232–1261. [[CrossRef](#)]
19. Lago, N.; Garcia-Calvo, O.; del Amo, J.M.L.; Rojo, T.; Armand, M. All-Solid-State Lithium-Ion Batteries with Grafted Ceramic Nanoparticles Dispersed in Solid Polymer Electrolytes. *ChemSusChem* **2015**, *8*, 3039–3043. [[CrossRef](#)]
20. Villaluenga, I.; Bogle, X.; Greenbaum, S.; de Muro, I.G.; Rojo, T.; Armand, M.J. Cation only conduction in new polymer–SiO<sub>2</sub> nanohybrids: Na<sup>+</sup> electrolytes. *Mater. Chem. A* **2013**, *1*, 8348–8352. [[CrossRef](#)]
21. Zhao, H.; Asfour, F.; Fu, Y.; Jia, Z.; Yuan, W.; Bai, Y.; Ling, M.; Hu, H.; Baker, G.; Liu, G. Plasticized Polymer Composite Single-Ion Conductors for Lithium Batteries. *ACS Appl. Mater. Interfaces* **2015**, *7*, 19494–19499. [[CrossRef](#)] [[PubMed](#)]
22. Porcarelli, L.; Shaplov, A.S.; Bella, F.; Nair, J.R.; Mecerreyes, D.; Gerbaldi, C. Single-Ion Conducting Polymer Electrolytes for Lithium Metal Polymer Batteries that Operate at Ambient Temperature. *ACS Energy Lett.* **2016**, *1*, 678–682. [[CrossRef](#)]
23. Schaefer, J.L.; Yanga, D.A.; Archer, L.A. High Lithium Transference Number Electrolytes via Creation of 3-Dimensional, Charged, Nanoporous Networks from Dense Functionalized Nanoparticle Composites. *Chem. Mater.* **2013**, *25*, 834–839. [[CrossRef](#)]
24. Bashiri, P.; Rao, T.P.; Naik, V.M.; Nazri, G.A.; Naik, R. AC conductivity studies of polyethylene oxide-garnet-type Li<sub>7</sub>La<sub>3</sub>Zr<sub>2</sub>O<sub>12</sub> hybrid composite solid polymer electrolyte films. *Solid State Ion.* **2019**, *343*, 115089. [[CrossRef](#)]
25. Brogioli, D.; Langer, F.; Kun, R.; la Mantia, F. Space-Charge Effects at the Li<sub>7</sub>La<sub>3</sub>Zr<sub>2</sub>O<sub>12</sub>/Poly(ethylene oxide) Interface. *ACS Appl. Mater. Interfaces* **2019**, *11*, 11999–12007. [[CrossRef](#)]
26. Choi, J.-H.; Lee, C.-H.; Yu, J.-H.; Doh, C.-H.; Lee, S.-M. Enhancement of ionic conductivity of composite membranes for all-solid-state lithium rechargeable batteries incorporating tetragonal Li<sub>7</sub>La<sub>3</sub>Zr<sub>2</sub>O<sub>12</sub> into a polyethylene oxide matrix. *J. Power Sources* **2015**, *274*, 458–463. [[CrossRef](#)]
27. He, K.; Chen, C.; Fan, R.; Liu, C.; Liao, C.; Xu, Y.; Tang, J.; Li, R.K.Y. Polyethylene oxide/garnet-type Li<sub>6.4</sub>La<sub>3</sub>Zr<sub>1.4</sub>Nb<sub>0.6</sub>O<sub>12</sub> composite electrolytes with improved electrochemical performance for solid state lithium rechargeable batteries. *Compos. Sci. Technol.* **2019**, *175*, 28–34. [[CrossRef](#)]
28. Huang, Y.; Ma, M.; Guo, Y.J. Melt crystallization and segmental dynamics of poly(ethylene oxide) confined in a solid electrolyte composite. *Polym. Sci.* **2020**, *58*, 466–477. [[CrossRef](#)]
29. Langer, F.; Kun, R.; Schwenzel, J. *Li<sub>7</sub>La<sub>3</sub>Zr<sub>2</sub>O<sub>12</sub> and Poly(Ethylene Oxide) Based Composite Electrolytes*; Springer: Cham, Switzerland, 2019.
30. Langer, F.; Palagonia, M.S.; Bardenhagen, I.; Glenneberg, J.; la Mantia, F.; Kun, R.J. Impedance Spectroscopy Analysis of the Lithium Ion Transport through the Li<sub>7</sub>La<sub>3</sub>Zr<sub>2</sub>O<sub>12</sub>/P(EO)<sub>20</sub>Li Interface. *Electrochem. Soc.* **2017**, *164*, A2298–A2303. [[CrossRef](#)]
31. Li, Z.; Huang, H.M.; Zhu, J.K.; Wu, J.F.; Yang, H.; Wei, L.; Guo, X. Ionic Conduction in Composite Polymer Electrolytes: Case of PEO:Ga-LLZO Composites. *ACS Appl. Mater. Interfaces* **2019**, *11*, 784–791. [[CrossRef](#)]
32. Samsinger, R.F.; Schopf, S.O.; Schuhmacher, J.; Treis, P.; Schneider, M.; Roters, A.; Kwade, A.J. Influence of the Processing on the Ionic Conductivity of Solid-State Hybrid Electrolytes Based on Glass-Ceramic Particles Dispersed in PEO with LiTFSI. *Electrochem. Soc.* **2020**, *167*, 120538. [[CrossRef](#)]

33. Zaman, W.; Hortance, N.; Dixit, M.B.; de Andrade, V.; Hatzell, K.B. Visualizing percolation and ion transport in hybrid solid electrolytes for Li–metal batteries. *J. Mater. Chem. A* **2019**, *7*, 23914–23921. [[CrossRef](#)]
34. Zheng, J.; Dang, H.; Feng, X.; Chien, P.-H.; Hu, Y.-Y. Li-ion transport in a representative ceramic–polymer–plasticizer composite electrolyte: Li<sub>7</sub>La<sub>3</sub>Zr<sub>2</sub>O<sub>12</sub>–polyethylene oxide–tetraethylene glycol dimethyl ether. *J. Mater. Chem. A* **2017**, *5*, 18457–18463. [[CrossRef](#)]
35. Zheng, J.; Tang, M.; Hu, Y.-Y. Lithium Ion Pathway within Li<sub>7</sub>La<sub>3</sub>Zr<sub>2</sub>O<sub>12</sub>-Polyethylene Oxide Composite Electrolytes. *Angew. Chem. Int. Ed.* **2016**, *55*, 12538–12542. [[CrossRef](#)] [[PubMed](#)]
36. Bernuy-Lopez, C.; Manalastas, W.; del Amo, J.M.L.; Aguadero, A.; Aguesse, F.; Kilner, J.A. Atmosphere Controlled Processing of Ga-Substituted Garnets for High Li-Ion Conductivity Ceramics. *Chem. Mater.* **2014**, *26*, 3610–3617. [[CrossRef](#)]
37. Li, Y.; Han, J.-T.; Wang, C.-A.; Xie, H.; Goodenough, J.B. Optimizing Li<sup>+</sup> conductivity in a garnet framework. *J. Mater. Chem.* **2012**, *22*, 15357–15361. [[CrossRef](#)]
38. Chen, Y.; Wen, K.; Chen, T.; Zhang, X.; Armand, M.; Chen, S. Recent progress in all-solid-state lithium batteries: The emerging strategies for advanced electrolytes and their interfaces. *Energy Storage Mater.* **2020**, *31*, 401–433. [[CrossRef](#)]
39. Zhang, Q.; Liu, K.; Wen, Y.; Kong, Y.; Wen, Y.; Zhang, Q.; Liu, N.; Li, J.; Ma, C.; Du, Y. Advances in solid lithium ion electrolyte based on the composites of polymer and LLTO/LLZO of rare earth oxides. *Eng. Rep.* **2022**, *4*, e12448. [[CrossRef](#)]
40. Queffelec, C.; Petit, M.; Janvier, P.; Knight, D.A.; Bujoli, B. Surface modification using phosphonic acids and esters. *Chem. Rev.* **2012**, *112*, 3777–3807. [[CrossRef](#)]
41. Rettenwander, D.; Wagner, R.; Reyer, A.; Bonta, M.; Cheng, L.; Doeff, M.M.; Limbeck, A.; Wilkening, M.; Amthauer, G. A Synthesis and Crystal Chemical Study of the Fast Ion Conductor Li<sub>7-3x</sub>Ga<sub>x</sub>La<sub>3</sub>Zr<sub>2</sub>O<sub>12</sub> with x = 0.08 to 0.84. *J. Phys. Chem. C* **2018**, *122*, 3780–3785. [[CrossRef](#)]
42. Bruce, P.G.; Vincent, C.A. Steady state current flow in solid binary electrolyte cells. *J. Electroanal. Chem. Interf. Electrochem.* **1987**, *225*, 1–17. [[CrossRef](#)]
43. Buannic, L.; Orayech, B.; del Amo, J.-M.L.; Carrasco, J.; Katcho, N.A.; Aguesse, F.; Manalastas, W.; Zhang, W.; Kilner, J.; Llordés, A. Dual Substitution Strategy to Enhance Li<sup>+</sup> Ionic Conductivity in Li<sub>7</sub>La<sub>3</sub>Zr<sub>2</sub>O<sub>12</sub> Solid Electrolyte. *Chem. Mater.* **2017**, *29*, 1769–1778. [[CrossRef](#)]